IEEE Access
Multidisciplinary ⋮ Rapid Review ⋮ Open Access Journal

Received 17 July 2023, accepted 7 August 2023, date of publication 14 August 2023, date of current version 17 August 2023.

Digital Object Identifier 10.1109/ACCESS.2023.3304647

RESEARCH ARTICLE

A Novel Differential Protection Scheme for Distribution Lines Under Weak Synchronization Conditions Considering DG Characteristics

WEI JIN[1,2], SHUO ZHANG[1], JIAN LI[1], MENGQIANG FENG[1], SHIGUANG FENG[1], AND YUPING LU[3], (Senior Member, IEEE)

[1]School of Electrical Engineering, China University of Mining and Technology, Xuzhou 221116, China
[2]Jiangsu Laboratory of Coal Mine Electrical and Automation Engineering, China University of Mining and Technology, Xuzhou 221116, China
[3]School of Electrical Engineering, Southeast University, Nanjing 210096, China

Corresponding author: Shuo Zhang (zs2001zs@163.com)

This work was supported in part by the Fundamental Research Funds for the Central Universities under Grant 2021QN1067, and in part by the China University of Mining and Technology for Experimental Technology Research and Development.

ABSTRACT A large number of DGs(distributed generators) in the ADN (active distribution network) bring great uncertainty to the power systems, making it difficult to quantify fault characteristics. Undoubtedly, the setting of traditional protection becomes more complex and difficult. Therefore, the differential protection is an effective solution to cope with it. However, the differential protection requires high time synchronization, which is difficult to be satisfied based on the current communication conditions of ADNs. What's more, accurate extraction of fundamental frequency components is also very difficult considering the distortion, the frequency offset, and the instability of fault currents. In view of this, a new differential protection scheme that makes full use of fault information is proposed in this paper. First, the pre-fault current waveforms are taken as reference. Then the similarity characteristics of the current waveform sequences at both terminals of the line are calculated separately. Finally, a new differential protection scheme considering weak synchronization conditions are constructed using Hausdorff distance, which is based on wide frequency components. The proposed scheme only transmits calculation results instead of sampling values, which effectively avoids the impact caused by data synchronization errors. Simulation shows that the proposed scheme can reliably identify internal faults in various points of the protected line and external faults. Compared with the conventional differential protections, it also shows great resistance to the transition resistance up to 30Ω, which is common in the ADN. Moreover, it has strong resistance to time synchronization errors, which can withstand time synchronization errors of up to 20ms. The proposed protection scheme has excellent engineering application value, especially suitable for distribution networks with weak communication conditions.

INDEX TERMS Active distribution network, differential protection, distributed generation, hausdorff distance, weak synchronization.

LIST OF ACRONYMS

ADN	Active distribution network.
CRF	Calculated result factor.
DG	Distributed generation.
DP	Differential protection.
FDSS	Fault data self-synchronization.
IIDG	Inverter-interface DG.
LVRT	Low voltage ride through.
MPPT	Maximum power point tracking.
PV	Photovoltaic.
SCADA	Supervisory Control and Data Acquisition.
TTCAF	Two terminals current amplitude factor.

The associate editor coordinating the review of this manuscript and approving it for publication was Qiang Li.

This work is licensed under a Creative Commons Attribution-NonCommercial-NoDerivatives 4.0 License.
For more information, see https://creativecommons.org/licenses/by-nc-nd/4.0/

I. INTRODUCTION

With the deteriorating ecological environment and gradually severe energy crisis, the renewable energy represented by wind and solar energy has been rapidly developed and widely used in China. As a result, the energy structure is undergoing significant changes, providing important guarantees and support for achieving the ''30-60'' carbon peaking and carbon neutrality goals. As of January 2021, the total new energy generation in China has exceeded 1 trillion kWh, and the total new energy generation for the year 2021 accounts for 13.8% of the national electricity consumption. According to the 14th Five-Year Plan of the National Energy Administration, there is no doubt that renewable energy will be further developed, and the traditional distribution grid will gradually develop into a new distribution grid system with high penetration of DGs [1], [2]. However, the access of DGs have transformed the distribution network from traditional radial power supply system to multi-ended one, changing the magnitude and direction of fault currents in the feeder lines. As a result, some protection schemes deployed in traditional distribution networks like three-stage overcurrent protection may malfunction in some cases [3], [4], [5], [6], [7]. According to the technical standard for DGs connected to power grid, reactive current should be output in priority to support the system voltage after a fault occurs [8], hence the phase and amplitude of the output current supplied by the DG has significant randomness, which is related to the pre-fault operating state, fault type, the degree of voltage dip, etc. Obviously, the performance of protection is affected. More seriously, in case of DGs disconnected from the grid after a fault, the changes in the topology of the distribution network can also have adverse effects on traditional relay protection [9]. Therefore, in order to promote the development of the ADN, it is imperative to propose a suitable distribution network protection scheme to cope with the performance degradation of traditional relay protection in the ADN.

To address the problems brought by the integration of large-scale DGs into the distribution networks, the differential protections (DPs) are increasingly used in the distribution network [10], [11], [12], [13], [14], [15], [16], [17]. The Kirchhoff's Current Law-based DP with proper parameter settings can accurately remove all kinds of internal faults, which does not require the coordination of the setting value and time delay between upper and lower-level protections and has good selectivity. What is more, due to the low voltage level of the feeder lines in the distribution network, the adverse effects brought by the capacitor charging current of the line are smaller compared to the transmission system, making it more advantageous for the application of differential protection in distribution networks.

But conventional DP requires strict synchronization of data at both terminals of the line. However, due to the large scale of the distribution network, the economic issues must be considered whenever the differential protection is claimed for the distribution networks [18], which hinder the promotion and application of the DP in the distribution networks.

The main solutions to the application of DP in distribution networks include improving the communication conditions in the distribution networks, proposing differential protection scheme with lower requirements for data synchronization and proposing fault data self-synchronization (FDSS) algorithms for DP. A distribution network current differential protection based on 5G wireless communication is proposed in [19] to achieve full line quick action for phase-phase short circuit faults in distribution networks under various operation modes. But the status quo of the distribution network is difficult to meet high synchronous communication conditions, and upgrading and renovating the equipment of the distribution network will bring great construction and renovation costs. The differential protection criterions for distribution networks based on the amplitude ratio of currents on both sides are proposed in [20] and [21]. These types of protection scheme do not require strict data synchronization due to the main impact of asynchronous data on current phase rather than amplitude, but the effectiveness of such protection schemes have restrictions on the penetration rate of DGs. The proposed schemes may fail if the fault points is close to the DGs at downstream. In [22], a positive sequence differential impedance criterion is constructed by analyzing the characteristic differences of positive sequence differential impedance between internal and external faults in the protected section. A distribution network DP based on impedance information is proposed in [23] and [24], which has strong resistance to synchronization errors. Unfortunately, potential transformers are not usually available at each bus in medium and low voltage distribution grids, which limits the application of the above-mentioned method that require voltage measurement, so the promotion and application of such methods are districted. The regional current direction based protection method in the ADN is proposed in [25], which determines the fault location by the relationship between current direction and current amplitude. However, due to the randomness of the DG output current, it is not possible to accurately identify the fault location when the DG output changes. Some scholars propose FDSS algorithm for DP deployed in ADN to reduce reliance on synchronous communication [26], but the algorithm will have a large time synchronization error under some extreme fault conditions, consequently reducing the reliability of DP. The DP criterion based on FDSS which utilizes time information is also proposed in [27] to solve the time synchronization in distribution networks, but high accuracy in information transmission is still required. Current Solutions to promote the applications of DP in distribution networks are listed in Table 1.

Obviously, the uncertainty brought by a large number of DGs connected to the distribution network makes it difficult to quantify the fault characteristics. What's more, data transmission and synchronization in distribution networks is often achieved by multiplexing SCADA channels nowadays. Due to the large network structure and numerous nodes of the distribution network, laying dedicated channels for data transmission is not economical enough. The data transmission

TABLE 1. Current solutions to application of DP in distribution networks.

Solutions	Disadvantages
Improve the communication conditions	High cost for update of distribution network
Propose protection schemes with lower data synchronization requirements	They may malfunction in some cases or the applications of them are limited by the status quo of the ADNs
Propose FDSS algorithms for DP	There will be a large time synchronization error under some extreme fault conditions

by the way of multiplexing SCADA channels can meet the needs of data transmission, so it has been applied in distribution networks. But for data synchronization, there may be inconsistent data transmission and reception delays when the distribution network multiplexes SCADA channels for communication, which affects the timing accuracy of communication channel-based synchronization methods [28]. So the ADN also faces problems such as the low automation level and the weak synchronous communication capability at both terminals of the line. Some scholars propose protection schemes based on waveform similarity are mainly for transmission systems, and most of them are based on two-terminal sampling values for comparison [29], [30], [31], [32], so the problem of data synchronization at both terminals of the protected lines still needs to be considered. Therefore, in order to solve the problems above, a new differential protection scheme that does not rely on the fundamental frequency component but fully utilizes fault information is proposed in this paper. Firstly, taking the pre-fault waveform as reference, the differences between the pre-fault and post-fault current waveforms at both terminals of the line are analyzed respectively based on the fact the pre-fault current at two terminals of the line is same. Then, in view of the same characteristics of the pre-fault waveform, the similarity characteristics between the current waveform sequences at both ends of the line are indirectly calculated based on the Hausdorff distance principle. Finally, the differential protection criterion under weak synchronization conditions considering various factors is constructed in this paper. The operation performance of the proposed protection scheme under various types of faults and weak time synchronization is illustrated based on a typical 10 kV ADN simulation system. Simulations show that the proposed protection scheme has high accuracy, sensitive operation for internal faults, reliable braking for external faults, good resistance to transition resistance, and good resistance to synchronization errors.

II. ANALYSIS OF FAULT CURRENT CHARACTERISTICS

The widely used Inverter-interface DGs (IIDG), controlled by flexible power electronic components, can effectively improve the reliability of power supply in ADNs due to its outstanding power conversion capability [33], [34]. According to the technical requirements for grid connection of distributed resources, the DGs must have LVRT (low voltage ride through) capability to ensure the safe and stable operation of the power grid during a fault. Therefore, when the grid voltage drops during a fault, DG must output reactive current to support the grid voltage. At the same time, in order to maintain the balance of active power, DG should output active current as much as possible during a fault. Taking distributed PV power generation as an example, the post-fault active current, post-fault reactive current of DG can be written as followed,

$$\begin{cases} I_d = \min[\sqrt{I_{\max}^2 - I_q^2}, \frac{P_{ref}}{U_{PCC}}] \\ I_q = \begin{cases} K_1 I_N & U_T < 0.2 \\ K_2(0.9 - U_T) & 0.2 \le U_T \le 0.9 \\ 0 & U_T > 0.9 \end{cases} \end{cases} \tag{1}$$

where K_1, K_2 are the voltage support factors respectively and $K_1 \geq 1.05$, $K_2 \geq 1.5$, I_N the PV rated current, U_T the PV terminal voltage unit value, $I_{\max}$ the maximum allowable output current of distributed PV inverter, P_{ref} the active power reference value of PV, U_{PCC} the voltage at the PCC(point of common coupling)

Then the angle α of the distributed PV output current lagging behind the voltage at the PCC after the fault [4] can be written as

$$\alpha = \arctan \frac{I_q}{I_p} \tag{2}$$

where I_p, I_q are the post-fault active and reactive currents output by DG, respectively.

I_p, I_q are mainly affected by the severity degree of voltage dips, which are related to various factors such as fault location, fault type, and transition resistance. The DG terminal voltage is uncertain after the fault, so the phase of the post-fault DG output current is random. Since the voltage dips are affected by various factors such as the location of the fault occurrence, the type of fault, and the size of the transition resistance, the voltage at the parallel network after the fault is uncertain, so the phase of the DG output current after the fault has a large randomness, which may lead to the possible misjudgment of the directional components of the protection. In order to ensure the reliability of the protection, it is necessary to select the state quantity that is less affected by the DG operation state and can reflect based on the DG fault characteristics more obviously to construct the protection scheme. In general, the system side capacity is much larger than the DG side, and influenced by the control strategy of DG, the short-circuit current provided by DG is usually much smaller than the short-circuit current provided by the system, and The current magnitude difference between the system side, and DG side before and after the fault is obvious, so it is reasonable to analyze the fault characteristics of the system based on the current amplitude. The fault characteristics of the system should be analyzed from the perspective of current magnitude.

As is shown in Figure 1, the schematic diagram of a typical ADN specifies that the positive direction of the current is from the bus to the line.

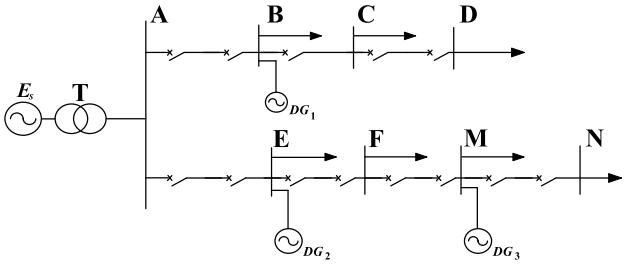

FIGURE 1. Typical topology of active distribution network.

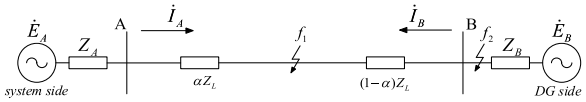

FIGURE 2. Schematic diagram of active distribution network.

Taking line AB as an example, the multi-terminal equivalent diagram of the ADN after the DG is connected to the distribution network is shown in Figure 2.

First, assume that DG is a conventional power supply. When a three-phase short-circuit fault occurs at f_1, the A-side current and the B-side current can be written as in (3) respectively,

$$\begin{cases} \dot{I}_A = \frac{\dot{E}_A}{Z_A+\alpha Z_L} \\ \dot{I}_B = \frac{\dot{E}_B}{Z_B+(1-\alpha)Z_L} \end{cases} \tag{3}$$

where $\dot{E}_A$ is the system side equivalent power source, $\dot{E}_B$ is the DG side equivalent power source, Z_A is the system side equivalent internal impedance, Z_B is the DG side equivalent internal impedance, Z_L is the impedance of the line AB and α is the ratio of the line fault length (the length from the head end of the line to the fault location) to the line length.

Due to the low voltage level of the distribution network, the influence of the line to ground capacitor current can be ignored. When an external fault at f_2 occurs, a ride-through current flows both ends of line AB. According to the previously specified positive direction, the A-side current and B-side current are equal in magnitude and opposite in phase, which can be written as,

$$\dot{I}_A = -\dot{I}_B = \frac{\dot{E}_A - \dot{E}_B}{Z_A + Z_B + Z_L} \tag{4}$$

It is specified that η_A is the ratio of the pre-fault current and post-fault current at A side. η_A is written as,

$$\eta_A = \left|\frac{\dot{E}_A}{\dot{E}_A - \dot{E}_B}\right| \cdot \frac{|Z_A + Z_B + Z_L|}{|Z_A + \alpha Z_L|} \tag{5}$$

Similarly, η_B is written as,

$$\eta_B = \left|\frac{\dot{E}_B}{\dot{E}_A - \dot{E}_B}\right| \cdot \frac{|Z_A + Z_B + Z_L|}{|Z_B + (1-\alpha) Z_L|} \tag{6}$$

Defining the ratio η of η_A to η_B as the pre-fault and post-fault of two terminals current amplitude factor(TTCAF), then we have,

$$\eta = \frac{|\dot{E}_A|}{|\dot{E}_B|} \cdot \frac{|Z_B + (1-\alpha)Z_L|}{|Z_A + \alpha Z_L|} \tag{7}$$

Consider that the DG potential cannot be maintained for a long time during a fault, we have $|\dot{E}_A| > |\dot{E}_B|$. In addition, the system-side equivalent internal resistance Z_A is much smaller than the DG-side equivalent internal resistance Z_B. Therefore, it is clear that η decreases monotonically with α, and there is a minimum of η when $\alpha = 1$. Considering the most extreme case, when $\alpha = 1$, then we have,

$$\eta = \frac{|\dot{E}_A|}{|\dot{E}_B|} \cdot \frac{|Z_B|}{|Z_A + Z_L|} \tag{8}$$

The line length is generally within 20 kilometers and the line impedance is within 10Ω in the ADNs, so we always have $\eta > 1$. Obviously, the A-side amplitude ratio of post-fault and pre-fault current is quite different from the B-side amplitude ratio. Therefore, choosing the appropriate similarity calculation method can well describe the fault characteristics.

III. PROTECTION SCHEME BASED ON WIDE FRENQUENCY AMPLITUDE RATIO

Fundamental frequency component based protection schemes cannot effectively utilize the rich frequency components contained in the fault current in the ADNs [35]. Therefore, in order to make the protection scheme more adaptable and sensitive, extending the action criterion of the protection to a wider frequency domain is an effective solution. More fault characteristics can be included in the current sampling sequence, which contains a variety of frequency components Therefore, the protection scheme based on waveform similarity can fully utilize the fault characteristics of ADNs.

Hausdorff distance is a measure of similarity between two point sets. Let A and B be two subsets of the metric space M,

$$A = \{a_1, a_2, a_3, \cdots, a_p\} \tag{9}$$

$$B = \{b_1, b_2, b_3, \cdots, b_p\} \tag{10}$$

Define the Hausdorff one-way distance from set A to set B as

$$h(A, B) = \max_{a \in A} \min_{b \in B} \|a - b\| \tag{11}$$

Let $h(A, B) = \max\{h(A, B), h(B, A)\}$,then $h(A, B)$ is the Hausdorff distance between the set A and the set B.

The action speed of the fundamental frequency component-based protection scheme is constrained by the length of the data window of the protection algorithm. The Hausdorff distance algorithm is based on real-time similarity judgment of time-domain waveforms, so the length of the data window can be adaptively adjusted to meet different action speed requirements. Therefore, when there are few sampling points with a short data window, the computational complexity is small and the speed is fast. When the data window is long, the calculation result after a fault has less fluctuation and stronger tolerance for abnormal data [29], [30].

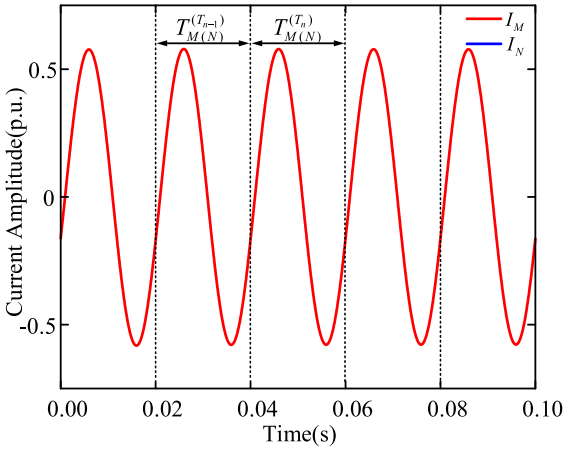

FIGURE 3. The M-side and N-side current waveforms under normal operation.

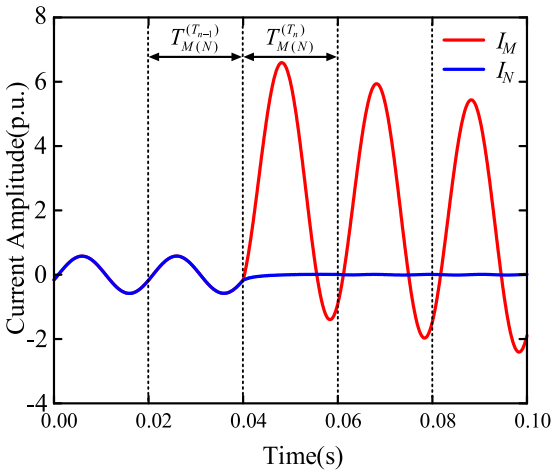

FIGURE 4. Schematic diagram of current waveform of two sides of the line in fault.

As shown in Figure 3, let $I_M^{(T_n)}$ and $I_N^{(T_n)}$ are sets of current sampling values of the M-side and N-side at a short time interval within the cycle T_n. Let $I_M^{(T_{n-1})}$ and $I_N^{(T_{n-1})}$ are sets of current sampling values of the M-side and N-side at the same time interval within the pre-cycle T_{n-1}. In case of the normal operation, the M-side and N-side current waveforms coincides with the current waveforms of the pre-cycle, respectively. Therefore, we have,

$$\begin{cases} h(I_M^{(T_{n-1})}, I_M^{(T_n)}) = 0 \\ h(I_N^{(T_{n-1})}, I_N^{(T_n)}) = 0 \end{cases} \tag{12}$$

As shown in Figure 4, when an internal fault occurs, the post-fault and pre-fault point set of the current sampling values differ significantly, and the similarity is poor, so we have,

$$\begin{cases} h(I_M^{(t-1)}, I_M^{(t)}) \gg 0 \\ h(I_N^{(t-1)}, I_N^{(t)}) \gg 0 \end{cases} \tag{13}$$

Define H_M as the similarity between the M-side post-fault the M-side pre-fault current, so we have $H_M = h(I_M^{(t-1)}, I_M^{(t)})$. Similarly, we have $H_N = H(I_N^{(t-1)}, I_N^{(t)})$. Obviously, in case of an external fault, we have $H_M/H_N = 1$. In case of an internal fault, we have $H_M/H_N > 1$ based on the TTCAF η mentioned above. Therefore, the Hausdorff distance can be used to express the similarity of the pre-fault current waveforms and post-fault current waveforms, and the ratio between them are used to construct a protection scheme to discriminate between internal and external faults.

The Hausdorff distance of each side can be calculated independently, which can be written as H_{qM} and H_{qN}, where H_{qM} is the M-side Hausdorff distance, and H_{qN} is the N-side Hausdorff distance. If $H_{qM} > \varepsilon$ (or $H_{qN} > \varepsilon$), the M-side (or N-side) protection device starts the fault diagnosis program, where ε is the activation threshold.

As shown in Figure 5, when the measured current reaches the activation threshold, the pre-fault current within $2T_0$ is

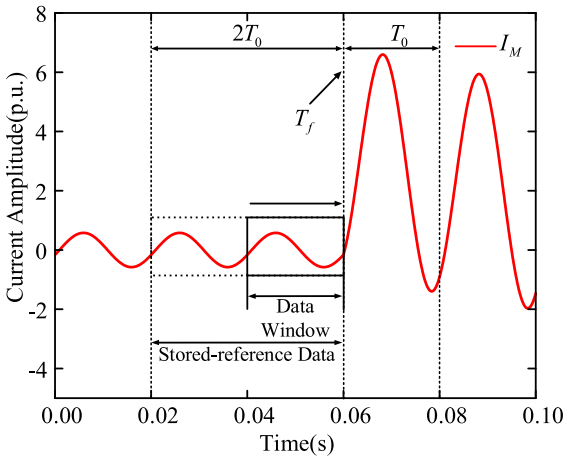

FIGURE 5. Schematic diagram of protection scheme at the head end of the line.

stored as the reference. Then the Hausdorff distances of the fixed time window between post-fault current and stored-reference current are calculated, respectively, which can be written as H_M and H_N. H_M/H_N and the action threshold K_0 satisfy the following relationship,

$$\frac{H_M}{H_N} > K_0 \tag{14}$$

Considering the time error in current sampling and the time delay during data transmission at both terminals, to ensure the reliability of the proposed protection scheme, it is considered that there is an internal fault when the inequality (14) is satisfied for more than the interval T_0. If the Hausdorff distance on the other side is not received or the inequality (14) is not satisfied, the protection devices automatically reset. In case of an internal fault, K_0 is set to 1.5 considering a certain margin and various errors. Considering the complexity of faults, in order to further improve the protection sensitivity of interval faults and the protection safety of external faults,

the adaptive function with the average value of the calculated result factor(CRF) $(H_M/H_N)_i$ is introduced to increase the action threshold in case of external faults and reduce the action threshold in case of internal faults. Then the improved protection criterion is written as,

$$\frac{H_M}{H_N} > K_0 f(aver(H_A/H_B)_i) + \varepsilon_0 \tag{15}$$

where ε_0 is the anti-malfunction threshold, $f(aver(H_A/H_B)_i)$ is a function on average value of CRF, namely $aver(H_A/H_B)_i$.

Furthermore, the function is $f(x) = 1/(1 + e^x)$ introduced to meet the above adaptive action threshold requirements [36], then $f(aver(H_A/H_B)_i)$ is written as,

$$f(aver(H_A/H_B)_i) = \frac{2}{1 + e^{aver(H_A/H_B)_i}} \tag{16}$$

where $aver(H_A/H_B)_i = \sum_{i=1}^{f_sT_0} (H_M/H_N)_i / (f_sT_0)$, f_s is the data window sampling frequency, T_0 is the post-fault fundamental frequency period of the current waveform, i is the index number of CRF. Substituting (16) into (15) yields,

$$\frac{H_M}{H_N} > \frac{3}{1 + e^{\left[\sum_{i=1}^{f_sT_0} \frac{(H_M/H_N)_i}{f_sT_0} - 1\right]}} + 0.5 \tag{17}$$

The proposed improved protection performance is determined by $aver(H_A/H_B)_i$. When an external fault occurs, if $\forall i \in [1, f_sT_0]$, then $(H_A/H_B)_i = 1$, so we have $aver(H_A/H_B)_i = 1$. Therefore, it is clear that $f(aver(H_A/H_B)_i) = 1$, and the action threshold is $K_0 + \varepsilon_0$, higher than the post-fault CRFs within T_0. As a result, the protection device of each side does not act on tripping. When the internal fault occurs, the value of $aver(H_A/H_B)_i$ becomes very large, therefore the adaptive threshold is reduced and the action area is increased to ensure the reliable action of the protection. The discrimination procedure for the proposed protection scheme is as followed based on the discussion above,

1) The pre-fault sampling data within $2T_0$ at two terminals of the protected line is stored as reference after the protection is activated.

2) Calculate Hausdorff distance of one terminal of the protected line between real-time sampling data within f_sT_0 after fault and 40ms pre-fault reference sampling data in 20ms data window point-by-point.

3) If one terminal always gets the CRF from the other one within f_sT_0 after fault, then the adaptive action threshold will be calculated based on the equation (17), otherwise the protection will be reset.

4) The protection will act if the CRFs always meet equation (17) more than 20ms, otherwise the protection will be reset.

The flowchart of the protection scheme is shown in the Fig 6.

Due to the poor communication conditions of the distribution network, it is difficult to synchronize the data between

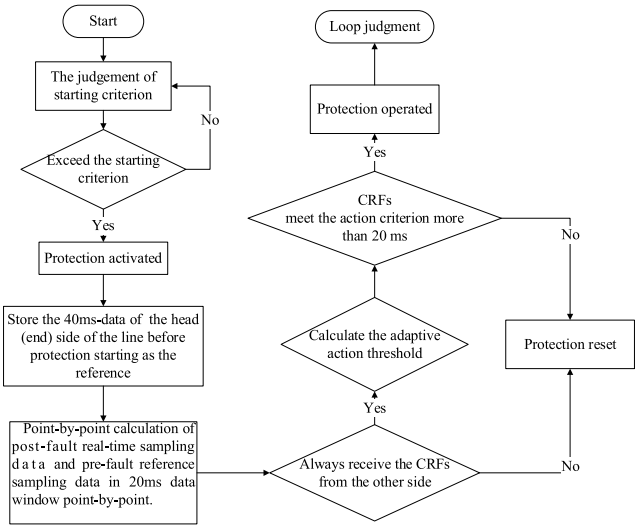

FIGURE 6. The flowchart of the protection scheme.

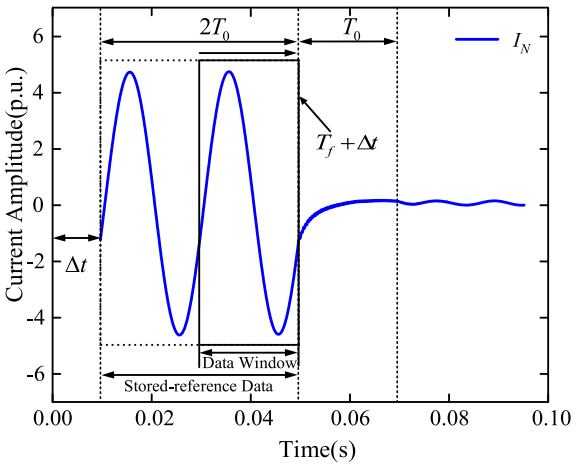

FIGURE 7. Diagram of weak synchronous communication between two sides.

the two sides of the line. As shown in Figure 7, the communication between the two sides of the line has a delay time of Δt. Let the moment of fault detection at the first side be T_f, and the other side be $T_f + \Delta t$. therefore. H_M is calculated by using the reference data from $T_f - 2T_0$ to T_f and the post-fault data from T_f to $T_f + 2T_0$, while H_N is calculated by using the reference data from $T_f - 2T_0 + \Delta t$ to $T_f + \Delta t$ and the post-fault data from $T_f + \Delta t$ to $T_f + 2T_0 + \Delta t$. Next, H_M and H_N are transmitted to the protection device on the opposite side to determine whether it is an internal fault. The protection scheme calculates the Hausdorff distance between pre-fault and pos-fault of the current waveform at both sides respectively. Because the proposed scheme only transmits calculation results instead of sampling values, which effectively avoids the impact caused by data synchronization errors.

The DG-connected distribution networks pose the great challenges to the time setting of the traditional three-stage

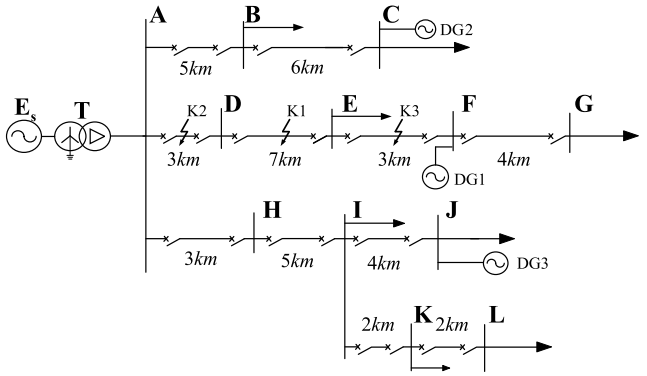

FIGURE 8. The topology of the ADN simulation system.

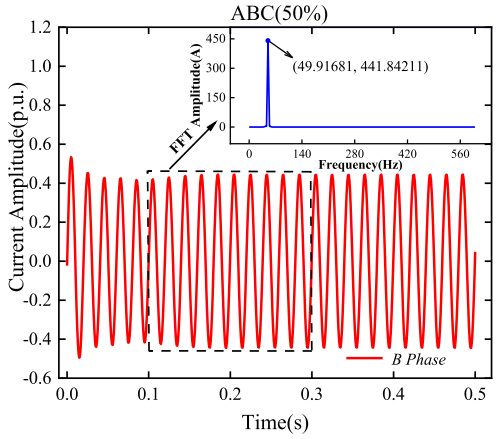

(a) The frequency spectrum of normal-operation current waveform at two sides of the line DE.

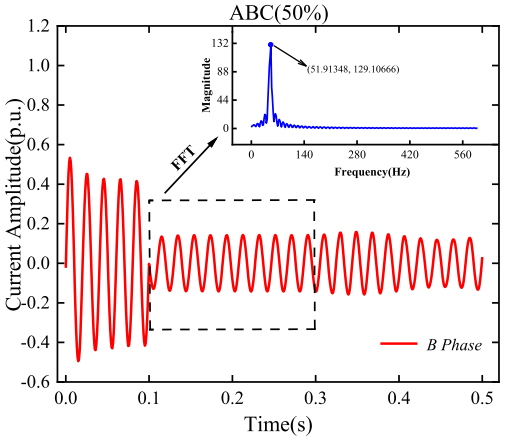

(b) The frequency spectrum of faulted current waveform at the end side of the line DE.

FIGURE 9. The frequency spectrums of normal-operation and faulted current waveform of the line DE.

overcurrent protection which is the most widely used in the distribution networks nowadays. The proposed protection scheme can be used as the alternative to the first and the second section of overcurrent protection. It is undeniable that there is still a risk of protection failure in rarely extreme cases due to the problems such as signal noise and CT transmission characteristics, etc. Since the current always rises sharply

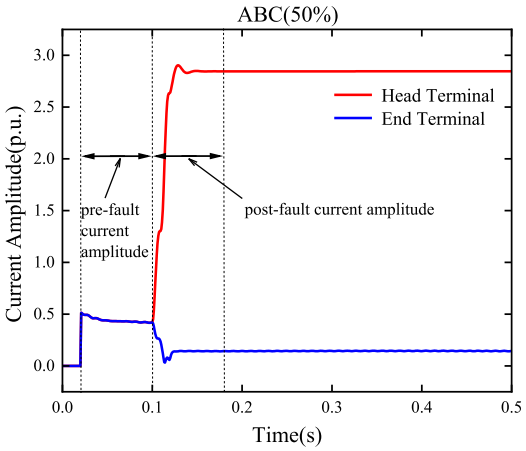

FIGURE 10. The current amplitude of two sides of the line DE in case of three- phase fault.

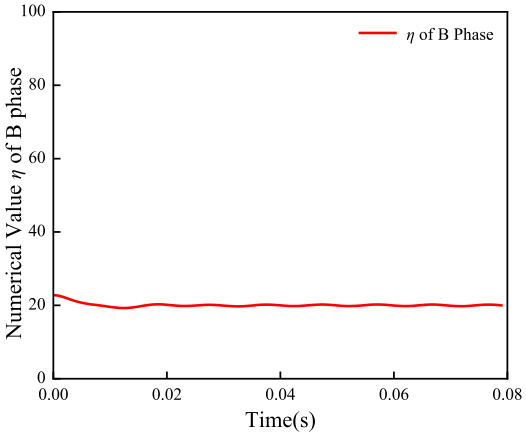

FIGURE 11. Numerical value of η of B phase.

when a short-circuit fault occurs in the distribution network line, the time-limited overcurrent protection can be used as a backup protection for the protection scheme proposed in this paper. The start and rest of the protection device is achieved through an overcurrent relay with the start current of I_{act}, which is written as (18),

$$I_{act} = \frac{K_{rel} K_{Ms}}{K_{re}} I_{L.\max} \tag{18}$$

where K_{rel} is the reliability coefficient, and its value is 1.25. K_{Ms} is the self starting coefficient and its value is 1.8. K_{re} is the is the self starting coefficient and its value and its value is 0.9. $I_{L.\max}$ is the maximum load current during normal operation. Considering the coordination between protections, set the time delay of relay protection t_{set} as 1s.

IV. SIMULATION VERIFICATION

In order to show the performance of the proposed protection scheme, a 10kV typical topology of ADN based on Matlab/ Simulink is taken as an example. As shown in Figure 8, the system capacity is 500 MVA. DG1 and DG3 are photovoltaics

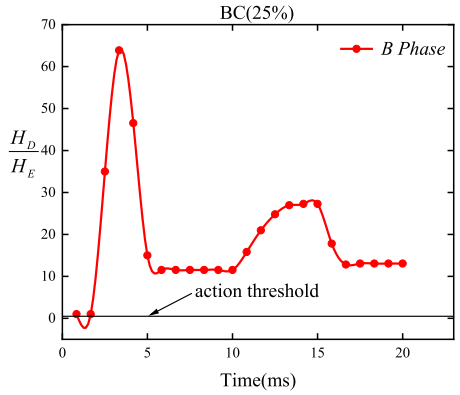

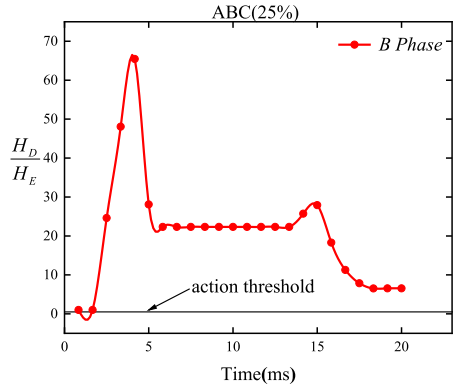

(a) Different types of fault at 25% of the length from the head of the line DE to the fault location.

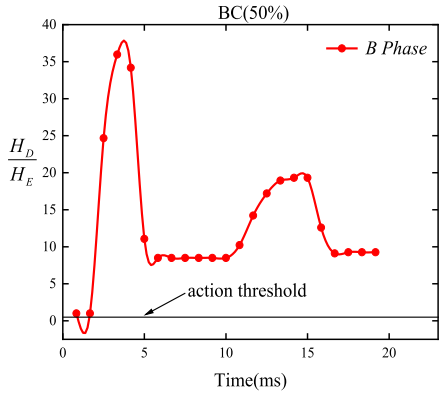

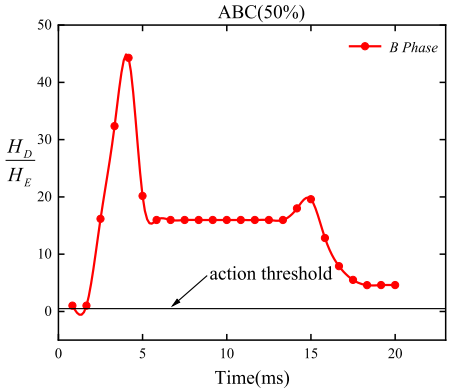

(b) different types of fault at 50% of the length from the head of the line DE to the fault location.

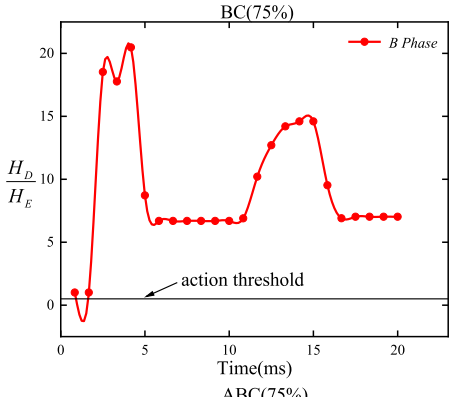

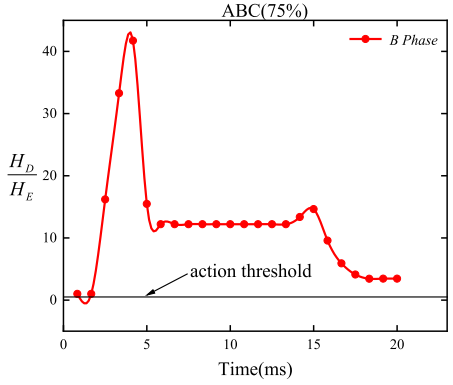

(c) Different types of fault at 75% of the length from the head of the line DE to the fault location.

FIGURE 12. Simulation results of internal faults under different types faults.

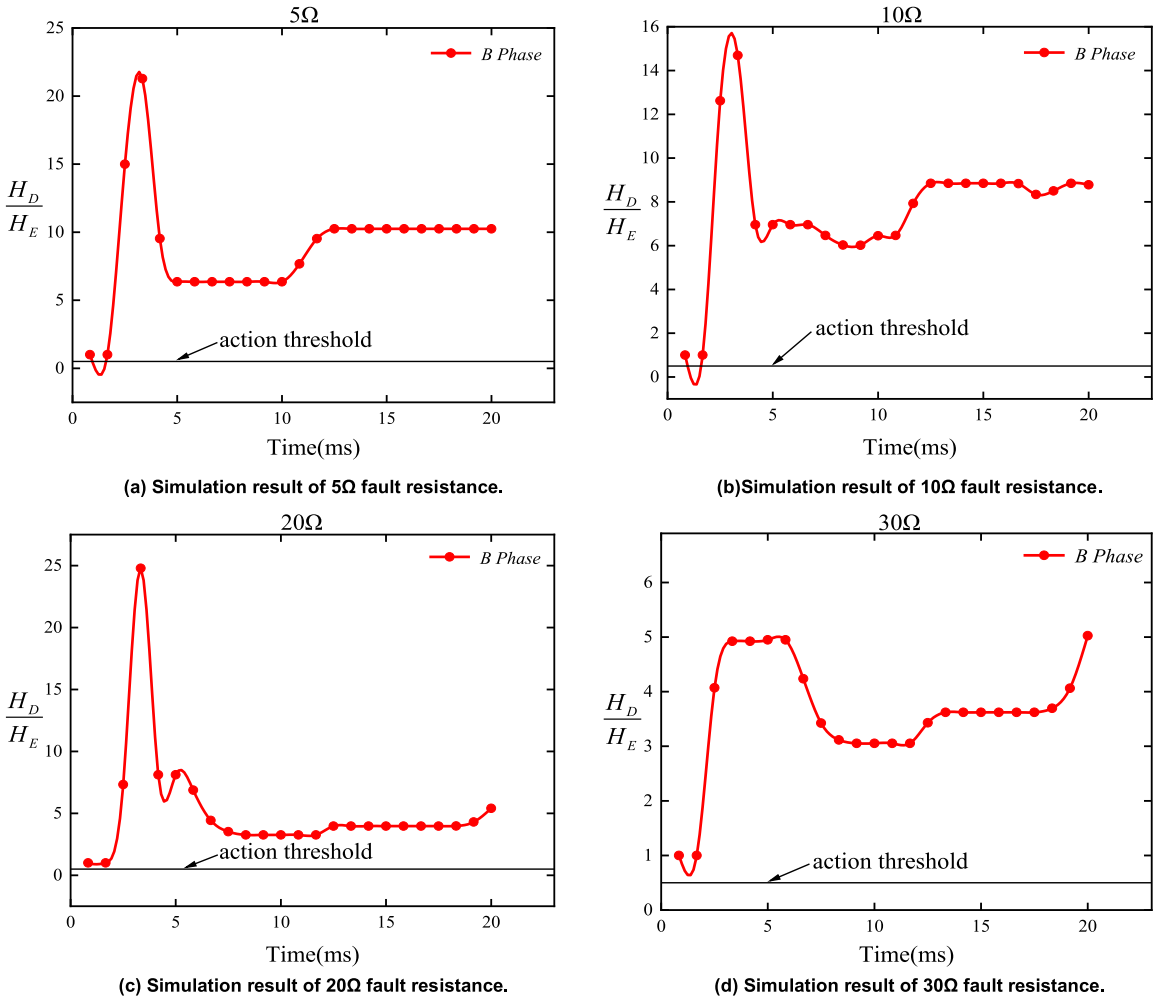

(a) Simulation result of 5Ω fault resistance.

(b)Simulation result of 10Ω fault resistance.

(c) Simulation result of 20Ω fault resistance.

(d) Simulation result of 30Ω fault resistance.

FIGURE 13. Simulation results of the traditional differential protection under phase-to-phase faults with different fault resistances.

(PV) with MPPT control strategy, and the power is 2MW at 1000 solar radiation intensity and 25°C ambient temperature. DG2 is DFIG distributed wind power with the power of 6MW at a wind speed of 15m/s. The unit line positive sequence impedance, zero sequence impedance is shown in Table 2. The data window length of the starting criterion is set to 5ms, and the data window length of the protection criterion is set to 20ms.

A. THE VERIFICATION OF FAULT FEATURES

According to the discussion above, take the line DE as the example for analysis. Fast Fourie Transform (FFT) is performed on the current waveform the line DE during normal operation and when a three-phase short circuit occurs to analyze wide frequency components, where the three-phase short circuit is set at 50% of the length from the head of the line DE. Essentially, Fourier transform analyzes signals by transforming time-domain signals into frequency-domain ones. In another words, the more frequency components are contained in the fault current, the more fault information is contained in the current time-domain waveform. The simulation time is 0.5s and the fault occurs at 0.1s. The frequency spectrums of normal-operation and faulty current waveform are shown in Figure 9.

As illustrated in Figure 9, when the three-phase short circuit occurs in the line DE, there is a frequency offset in the fault current, while the traditional differential protection works only based on the fundamental frequency, not fully utilizing fault information. Obviously, expanding protection to the wide frequency domain, namely constructing the protection criterion based on time-domain signals can make the protection criterion more representative and sensitive.

Moreover, the Figure 10 shows the current amplitude at both sides of the line DE during the simulation. Taking the pre-fault current amplitude form 0.02s to 0.1s and post-fault current amplitude from 0.1s to 0.18s as the example, the numerical value of TTCAF, namely η of B phase, as illustrated in Figure 11, is significantly greater than 1 in case of three-phase fault, which means great difference between pre-fault and post-fault current at two sides of the line.

TABLE 2. Parameters of simulation system.

Parameter	Value
Rated Voltage	10 kV
Capacity of Grid	500 MVA
Capacity of DG1	2 MW
Capacity of DG2	6 MW
Capacity of DG3	2 MW
Capacity of Loads	3.5 MVA
Positive sequence	$(0.17+1.36\times10^{-3})$ Ω/km
Zero sequence	$(0.23+3.87\times10^{-3})$ Ω/km

So it provides theoretical support for the proposed protection scheme and different fault scenarios will be set to verify the performance of the proposed protection scheme hereinafter.

B. THE EFFECT OF DIFFERENT FAULT TYPES

The fault locations are set as K1, K2 and K3, where K1 is the internal fault, and K2 and K3 are the external faults. K1 is set at 25%, 50% and 75% of the length from the head of the line DE to the fault location, respectively. K2 is 50% of the length from the head of the line AD to the fault location, and K3 is 50% of the length from the head of the line EF to the fault location. Taking the BC interphase short circuit and ABC three-phase short circuit of the DE section line as examples, they are recorded as BC and ABC, respectively. Set the simulation time as 0.5s and the fault moment as 0.2s after the start of the simulation and take the sampling data of the first two cycles before the occurrence of the fault, namely 0.16s to 0.20s, as the reference. The Hausdorff distance between the 20ms time window data and the reference data with a difference of k×20ms is calculated point by point and the 24 CRFs are obtained.

Figure 12 illustrates the B-phase results of the protection scheme when different types of faults occur at K1 with different locations.

As is shown in Figure 12, the CRFs of the proposed protection scheme is rapidly increased and maintained above the action threshold thereafter for internal faults in different locations, and the CRFs always satisfy the protection criterion. Simulations show that the proposed protection scheme can identify faults correctly in case of the internal faults of the protected line, and can reliably remove the fault with a trip signal if the calculation result exceeds the action threshold, which shows the reliability of the protection scheme.

The fault will be cleared by the backup protection if the proposed protection scheme fail to operate. The time-limited overcurrent protection will be activated after time delay t_{set}. As simulation results illustrated in TABLE 3, the backup protection can activate the protection devices and clear the internal faults at different locations after the time delay.

C. THE EFFECT OF TRANSITION RESISTANCE

Generally, there is a certain fault resistance during a fault. Therefore, taking fault at K2 point as an example, other simulation model parameters remain unchanged. Different fault resistances are set at the K2 to investigate the ability of the protection scheme to withstand the transition resistance.

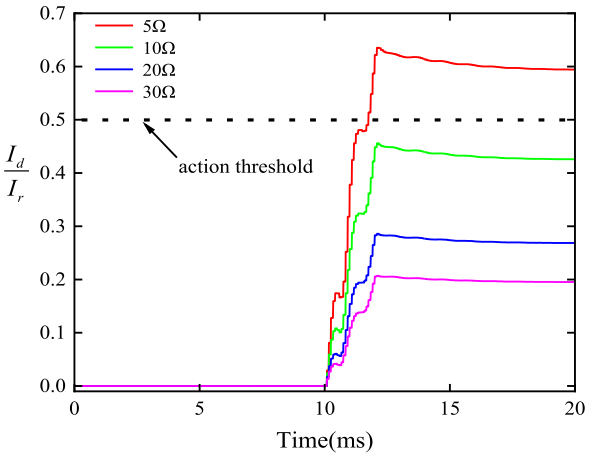

FIGURE 14. Simulation results of the traditional differential protection under phase-to-phase faults with different fault resistances.

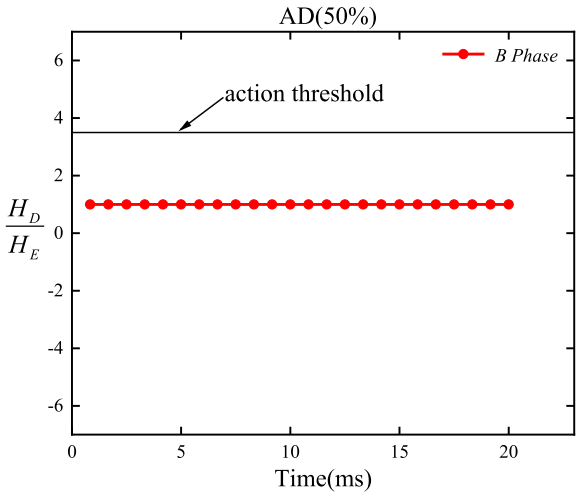

(a) Simulation result of the upstream fault.

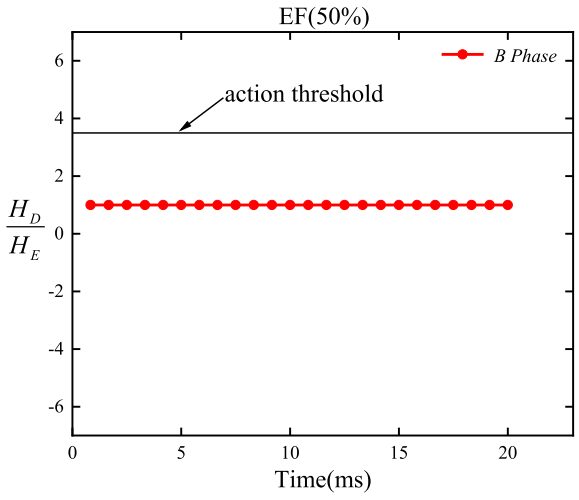

(b) Simulation result of the downstream fault.

FIGURE 15. Simulation results of protection scheme in case of external faults.

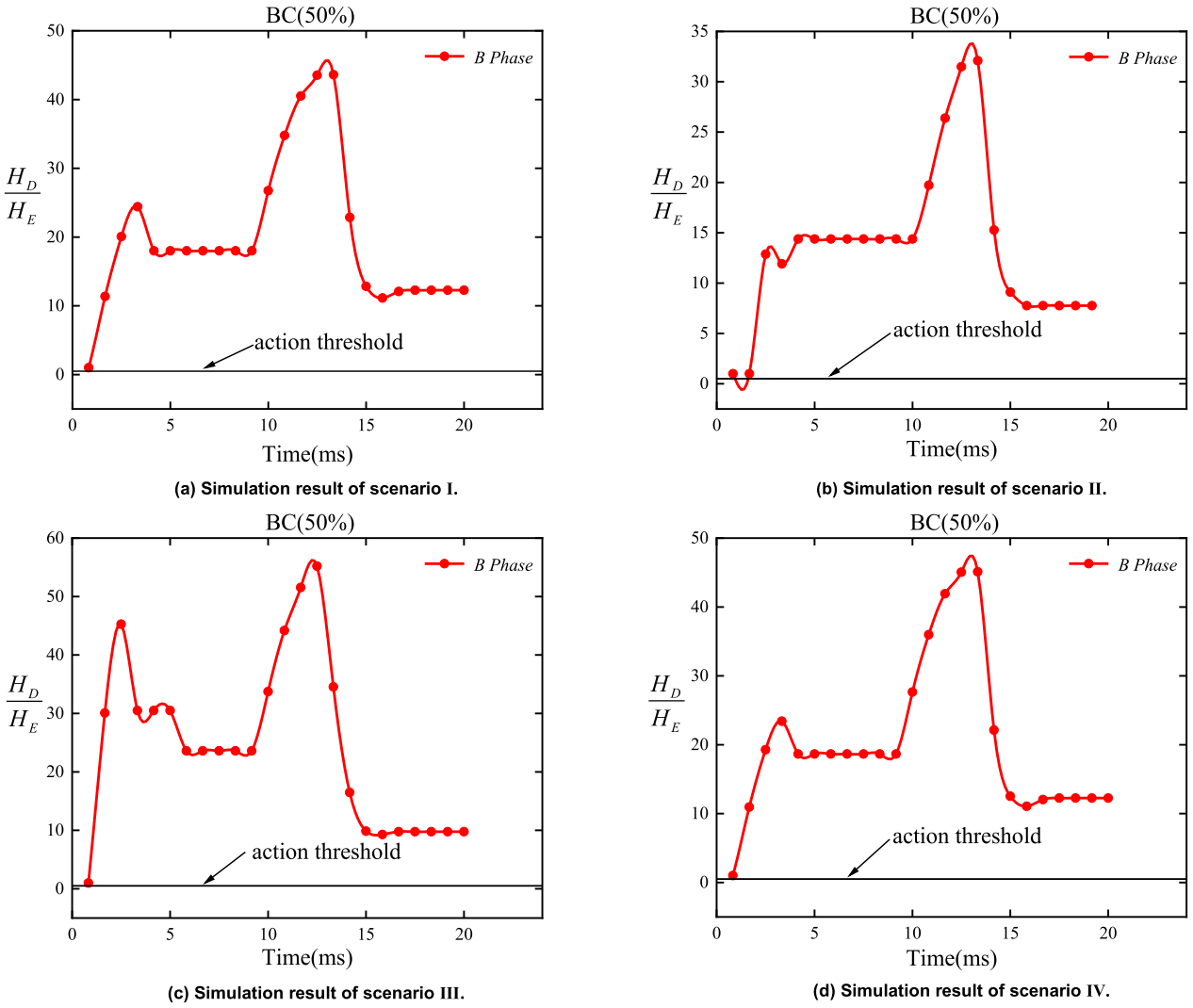

(a) Simulation result of scenario I.

(b) Simulation result of scenario II.

(c) Simulation result of scenario III.

(d) Simulation result of scenario IV.

FIGURE 16. Simulation results of different scenarios of DG1.

Since the transition resistance of 10 kV distribution network usually does not exceed 30Ω [36], 5Ω, 10Ω, 20Ω, and 30Ω fault resistances are set in the paper when the BC interphase short circuit occurs at K2. Taking phase B as an example, Figure 13 illustrates the CRFs of the protection scheme in case of BC interphase short circuit occurring at K2 with different transition resistances. It is shown that the CRFs gradually decrease as the resistance increases. The proposed protection scheme can still reliably identify the internal faults, therefore the protection principle has a certain ability to withstand the transition resistance.

The conventional differential protection has also been introduced to compare its performance with the proposed protection scheme in case of phase-to-phase fault with different fault resistance. The traditional differential protection criterion is written as (19),

$$\begin{cases} I_d \geq KI_r \\ I_d \geq I_{op.0} \end{cases} \tag{19}$$

TABLE 3. Simulation results of backup protection.

Fault Types	Fault Location	Fault Current(A)	I_{act}(A)
Phase to phase fault (BC)	25%	3814.826	1123.883
	50%	2845.203	
	75%	2268.905	
Three phase fault (ABC)	25%	3814.054	
	50%	2617.011	
	75%	2118.541	

where I_d is the differential current, $I_d = |\dot{I}_M + \dot{I}_N|$, and I_r is the braking current, $I_r = |\dot{I}_M - \dot{I}_N|$. $I_{op.0}$ is the minimum operating current. K is the braking coefficient and its typical value range is 0.5∼0.8 and in this paper it is set as 0.5.

As illustrated in Figure14, when the transition resistance increases, the ratio of differential current to braking current, I_d/I_r will be less than the braking coefficient, making it impossible to operate correctly in the case of an internal fault. It only operates under the phase-to-phase faults with the 5Ω

TABLE 4. Different operation scenarios of DG1.

Scenarios	Ambient temperature(°C)	Light intensity(W/m^2)
I	45	1500
II	25	200
III	25	500
IV	25	800

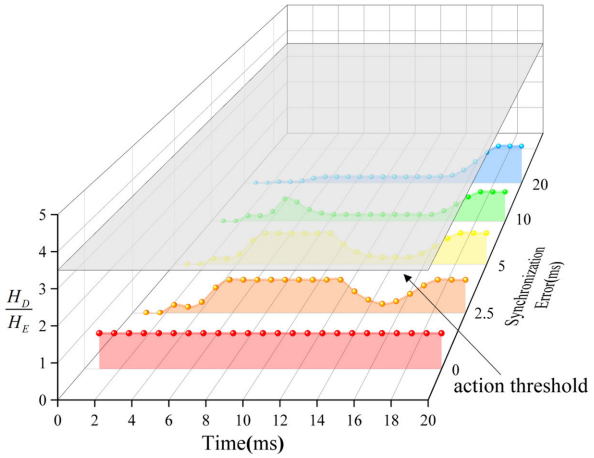

(a) Simulation results in case of external faults.

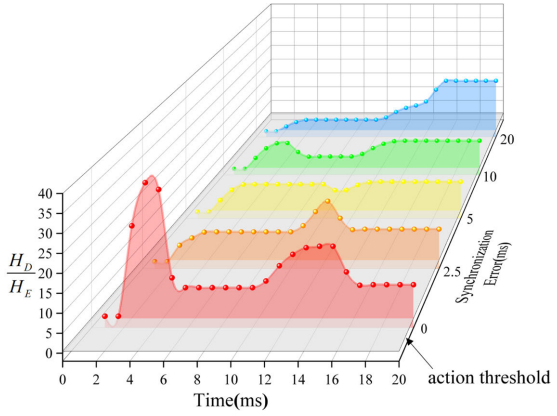

(b) Simulation results in case of internal faults.

FIGURE 17. Simulation results of protection scheme on internal and external faults under weak synchronization.

fault resistance in this simulation scenario. Obviously, the proposed protection scheme has excellent sensitivity.

D. THE EFFECT OF EXTERNAL FAULTS

In order to verify the reliability of the protection during the occurrence of the external fault, the type of BC interphase short-circuit fault is respectively set at K2 and K3 as shown in Figure 6 for verification, and the results of the protection scheme are shown in Figure 15.

As shown in Figure 15, when the BC interphase short-circuit fault is set at upstream and downstream of the protected line respectively, the through-fault current flows on the protected line, and the CRFs $(H_D/H_E)_i$ of the protected line with the proposed protection scheme remains around 1, which is lower than the adaptive action threshold of 3.5. Therefore, simulations show the high reliability of the proposed protection scheme during the occurrence of external faults.

E. THE EFFECT OF DIFFERENT OPERATION SCENARIOS OF DG

DG operation status is affected by weather and environment, and the power output is highly random. Take distributed PV as an example, its output current has a large volatility under different ambient temperature and light intensity. As shown in Table 4, this paper sets up different operation scenarios of DG1 to verify the reliability of the proposed protection scheme under the uncertainty of DG output, and Figure 16 shows the simulation results when the phase-to-phase short circuit occurs in line DE.

It can be seen that even when DG1 is operated under different scenarios, the CRFs of the proposed protection scheme are still larger than the action threshold within 20ms, which shows that the protection scheme has strong sensitivity and reliability.

F. ANALYSIS OF SYNCHRONIZATION ERRORS

The above analysis does not consider the problem of synchronization error of data measurement at both sides of the line. However, in the actual engineering application, it is difficult to achieve strict time synchronization of the sampled data at both terminals of the line. The faults are set in the line DE midpoint with BC two-phase short circuit, and line AD midpoint with BC two-phase short circuit, respectively. The time synchronization error of two-side sampling values is set 2.5ms, 5ms 10ms and 20ms, respectively.

As is shown in Figure 17, in the case of synchronization errors on both terminals of the protected line, the proposed protection scheme is still able to identify the internal faults. In case of external faults, the calculation results of the protection scheme show certain fluctuations compared to those without synchronization errors. However, the calculation results are still below the adaptive action threshold, which can ensure that the protection does not misoperation. Therefore, the protection scheme has good ability to resist synchronization error based on the analysis above.

V. CONCLUSION

A large number of DGs in the ADN bring great uncertainty to the power systems, which makes it difficult to quantify fault characteristics. Undoubtedly, the settings of traditional protection schemes become more complex and difficult. Therefore, the differential protection is an effective solution to cope with it. However, the differential protection requires high synchronization, which is difficult to be satisfied by the existing communication conditions of the distribution network. In addition, the distortion, the frequency offset, and the instability of fault signals also make it difficult to accurately extract the fundamental frequency component. Therefore, a new differential protection scheme that does not

rely on the fundamental frequency component is proposed in this paper. First, the pre-fault current waveforms are taken as reference. Then the similarity characteristics of the current waveform sequences at both ends of the line are calculated separately. Finally, the protection scheme considering weak synchronization conditions are constructed using Hausdorff distance, which is based on a wide range of frequency components rather than the fundamental frequency components. The following conclusions can be drawn from the theoretical analysis and simulation results,

1) The scheme proposed in this paper has good action performance and can act sensitively for different locations, different types of faults and common transition resistance in case of internal faults of the protected lines in the ADNs.

2) The protection scheme proposed in this paper calculates the similarity locally based on the pre-fault and post-fault current waveform, which does not require the transmission of dual ended sampling values. The proposed protection scheme does not require strict data synchronization and only requires the transmission of calculation results between both terminals, which is suitable for ADNs with low automation level and weak synchronous communication capability, and the proposed protection scheme can be used as the alternative to the first and the second section of overcurrent protection.

3) The scheme is proposed to address the application of differential protection in the distribution network, which is limited by the current poor communication conditions in the distribution networks. In the future, with the development of smart grid and the improvement of communication conditions, especially the application of new communication technology represented by 5G communication, it will greatly promote the application of differential protection in ADNs.

REFERENCES

[1] D. Ren, J. Xiao, J. Hou, E. Du, C. Jin, and X. Liu, "Construction and evolution of China's new power system under dual carbon goal," *Power Syst. Technol.*, vol. 46, no. 10, pp. 3831–3839, Jul. 2022.

[2] M. Barani, J. Aghaei, M. A. Akbari, T. Niknam, H. Farahmand, and M. Korpås, "Optimal partitioning of smart distribution systems into supply-sufficient microgrids," *IEEE Trans. Smart Grid*, vol. 10, no. 3, pp. 2523–2533, May 2019.

[3] Y. Zhu, "Study on sufficient current differential protection for distribution networks with wind power in weak synchronization condition," M.S. thesis, Dept. Elect. Eng., Southeast Univ., Jiangsu, China, 2019.

[4] Z. X. Wang, "Research on new type of current amplitude based differential protection for active distribution network," M.S. thesis, Dept. Elect. Eng., Huazhong Univ. Sci. Technol., Hubei, China, 2020.

[5] C. H. Zhou et al., "A pilot protection method based on positive sequence fault component current for active distribution networks," *Proc. CSEE*, vol. 40, no. 7, pp. 2102–2112, Mar. 2020.

[6] S. M. He et al., "Optimal setting method of inverse time over-current protection for a distribution network based on the improved grey wolf optimization," *Power Syst. Protection Control*, vol. 49, no. 18, pp. 173–181, Sep. 2021.

[7] Z. Y. He et al., "Key technologies for protection and control of novel urban power grids," *Proc. CSEE*, vol. 40, no. 19, pp. 6193–6207, Aug. 2020.

[8] D. H. Zeng et al., "Adaptive current protection scheme for distribution network with inverter-interfaced distributed generators," *Autom. Electr. Power Syst.*, vol. 41, no. 12, pp. 86–92, Jun. 2017.

[9] H. L. Weng et al., "Influence and countermeasures of distributed energy resources off-grid and its attribute change on line time limited current protection," *Proc. CSU-EPSA*, vol. 34, no. 10, pp. 1–8, Oct. 2022.

[10] X. Li and Y. Lu, "Improved amplitude differential protection scheme based on the frequency spectrum index for distribution networks with DFIG-based wind DGs," *IEEE Access*, vol. 8, pp. 64225–64237, 2020.

[11] B. Kara, F. Özveren, and Ö. Usta, "Protection of active distribution systems using differential relay," in *Proc. Nat. Conf. Electr., Electron. Biomed. Eng. (ELECO)*, Bursa, Turkey, Dec. 2016, pp. 53–57.

[12] B. Han, H. Li, G. Wang, D. Zeng, and Y. Liang, "A virtual multi-terminal current differential protection scheme for distribution networks with inverter-interfaced distributed generators," *IEEE Trans. Smart Grid*, vol. 9, no. 5, pp. 5418–5431, Sep. 2018.

[13] X. Miao, D. Zhao, B. Lin, H. Jiang, and J. Chen, "A differential protection scheme based on improved DTW algorithm for distribution networks with highly-penetrated distributed generation," *IEEE Access*, vol. 11, pp. 40399–40411, 2023.

[14] W. Li, Y. Tan, Y. Li, Y. Cao, C. Chen, and M. Zhang, "A new differential backup protection strategy for smart distribution networks: A fast and reliable approach," *IEEE Access*, vol. 7, pp. 38135–38145, 2019.

[15] H. Li and Y. Lu, "A novel sufficient differential protection for distribution network with DGs based on fault synchronous information," in *Proc. DRPT*, Changsha, China, 2015, pp. 858–863.

[16] M. Hossain, I. Leevongwat, and P. Rastgoufard, "Revisions on alpha plane for enhanced sensitivity of line differential protection," *IEEE Trans. Power Del.*, vol. 33, no. 6, pp. 3260–3262, Dec. 2018.

[17] H. L. Li, "Study on sufficient differential protection for distribution network with distributed generators based on fault synchronous identification technology," M.S. thesis, Dept. Elect. Eng., Southeast Univ., Jiangsu, China, 2016.

[18] A. Hooshyar and R. Iravani, "Microgrid protection," *Proc. IEEE*, vol. 105, no. 7, pp. 1332–1353, Jul. 2017.

[19] B. X. Dai, "Research on synchronization method of differential protection based on 5G wireless communication," in *Proc. POWERCON*, Haikou, China, 2021, pp. 2225–2228.

[20] Y. Gao et al., "Adaptive differential protection principle based on current amplitude ratio," *Proc. CSU-EPSA*, vol. 33, no. 2, pp. 1–7, 2021.

[21] X. S. Zhang et al., "Novel current amplitude differential protection criterion for line with unmeasurable branch in active distribution network," *Electr. Power Autom. Equip.*, vol. 40, no. 2, pp. 76–84, 2020.

[22] M. Xu, G. B. Zou, L. Gao, and Y. Ma, "Pilot protection of positive sequence impedance for distribution network with inverter-based distributed generator," *Autom. Electr. Power Syst.*, vol. 41, no. 12, pp. 93–98, 2017.

[23] C. X. Chao, X. D. Zheng, P. Gao, L. Tang, and Q. Tu, "High frequency impedance differential protection with high proportion of photovoltaic power distribution network," *Proc. CSEE*, vol. 41, no. 12, pp. 6968–6979, 2021.

[24] G. Chen, Y. Liu, and Q. Yang, "Impedance differential protection for active distribution network," *IEEE Trans. Power Del.*, vol. 35, no. 1, pp. 25–36, Feb. 2020.

[25] S. Zhao, T. Tang, D. Wang, R. Gao, and Z. Wu, "Active distribution network protection scheme based on area current direction," in *Proc. China Int. Electr. Energy Conf. (CIEEC)*, Beijing, China, Oct. 2017, pp. 247–251.

[26] H. Gao, J. Li, and B. Xu, "Principle and implementation of current differential protection in distribution networks with high penetration of DGs," *IEEE Trans. Power Del.*, vol. 32, no. 1, pp. 565–574, Feb. 2017.

[27] H. L. Li et al., "Sufficient differential protection for distribution network with distributed generators based on fault synchronous identification," *Autom. Electr. Power Syst.*, vol. 40, no. 11, pp. 100–107, Jun. 2016.

[28] J. Li, H. L. Gao, and X. Y. Gong, "A novel fault instant detection scheme for fault data self-synchronization method in distribution network," *Power Syst. Protection Control*, vol. 46, no. 4, pp. 92–98, Feb. 2018.

[29] L. Chen et al., "Waveform similarity comparison based high-speed pilot protection for transmission line," *Proc. CSEE*, vol. 37, no. 17, pp. 5018–5027 and 5221, Sep. 2017.

[30] Z. Rong, J. Neng, and L. Xiangning, "A novel criterion of adaptive busbar protection based on Hausdorff distance algorithm," *Power Syst. Technol.*, vol. 45, no. 1, pp. 312–321, Oct. 2021.

[31] Y. Hu, M. Zheng, K. Jia, H. Q. Li, and J. K. Zhang, "Pilot protection based on Tanimoto similarity for a photovoltaic station transmission line," *Power Syst. Protection Control*, vol. 49, no. 3, pp. 74–79, Feb. 2021.

[32] L. Zheng, K. Jia, T. Bi, Y. Fang, and Z. Yang, "Cosine similarity based line protection for large-scale wind farms," *IEEE Trans. Ind. Electron.*, vol. 68, no. 7, pp. 5990–5999, Jul. 2021.

[33] M. Ding, H. Di, and B. Rui, "Reliability analysis of distribution system containing high penetration renewable energy," *Acta Energiae Solaris Sinica*, vol. 41, no. 2, pp. 194–202, Feb. 2020.
[34] C. Li, "Research on protection scheme in active distribution network," M.S. thesis, Dept. Elect. Eng., North China Electr. Power Univ., Beijing, China, 2016.
[35] W. Jin, "Study on interaction mechanism of uncertain weak-feed sources in wind farms and relay protection," Ph.D. dissertation, Dept. Elect. Eng., Southeast Univ., Jiangsu, China, 2020.
[36] Y. Y. Liang and Z. J. Lu, "Adaptive differential protection principle based on compensation coefficient for active distribution network," *Autom. Electr. Power Syst.*, vol. 46, no. 6, pp. 2268–2275, Nov. 2022.

WEI JIN received the B.E. degree from Hehai University, Nanjing, China, in 2011, and the Ph.D. degree from Southeast University, Nanjing, in 2020. He is currently a Lecturer with the School of Electrical Engineering, China University of Mining and Technology. His research interests include power system protection in distribution systems with DGs and power systems optimization and modeling in energy interconnection.

SHUO ZHANG received the B.S. degree from the Huaiyin Institute of Technology, in 2022. He is currently pursuing the master's degree with the School of Electrical Engineering, China University of Mining and Technology. His research interests include active distribution network protection and power systems optimization and operation.

JIAN LI received the B.S. degree from the China University of Mining and Technology, in 2022. He is currently pursuing the master's degree in electrical engineering with the China University of Mining and Technology. He has engaged in the research on protection of power systems and power systems optimization and operation.

MENGQIANG FENG received the B.S. degree from the China University of Mining and Technology, in 2021. He is currently a Graduate Student with the School of Electrical Engineering, China University of Mining and Technology. He has engaged in research on power system relay protection and optimal power system operation.

SHIGUANG FENG received the B.S. degree from the Suzhou University of Science and Technology, in 2021. He is currently pursuing the master's degree with the School of Electrical Engineering, China University of Mining and Technology. He has engaged in the research on the line protection of the ac–dc hybrid power grids.

YUPING LU (Senior Member, IEEE) was born in Danyang, China, in October 1962. He received the Ph.D. degree in electrical engineering from the City University, U.K., in 2003. He is a Professor with Southeast University, China. His research interests include power system protection, especially digital relaying of generator-transformer units and protection and control techniques in distribution systems with DGs.

He is a member of the Technical Committee on Intelligent Power and Energy System. He severs as a Reviewer for the *International Journal of Power and Energy Systems*, IEEE PES TRANSACTIONS ON POWER DELIVERY.